Taylor & Francis
Taylor & Francis Group

Effect of Acetic Acid on CO_2 Corrosion of Carbon Steel in Vapor-Water Two-Phase Horizontal Flow

P. C. OKAFOR AND S. NESIC

Institute for Corrosion and Multiphase Flow Technology, Chemical Engineering Department, Ohio University, Athens, Ohio

The effect of acetic acid on the corrosion behavior of X 65 and C 1018 carbon steel in vapor-water two-phase stratified flow (Vsg: 2 m/s; Vsl: 0.1 m/s) at 2 bars total pressure, 1.54 bars CO_2 partial pressure, pH 5.5, and 80°C was studied in a low pressure-high temperature multiphase flow horizontal loop using electrochemical and mass loss techniques. The liquid phase is composed of 1% NaCl aqueous solution containing different concentrations of acetic acid (500 to 5000 ppm total acetic acid), and the gas phase is composed of CO_2-acetic acid-water vapor mixture. The corrosion rates, on both the top and bottom of the line, increase with increase in acetic acid concentration, which was attributed to the contribution of hydrogen ions by the free acetic acid to the cathodic reaction. Partial coverage of the metal surface by $FeCO_3$ on both the top and bottom of the line is reported to be responsible for the observed localized corrosion. Surface analysis investigated with SEM and XRD is reported.
A vapor-liquid equilibrium model was developed for the system studied.

Keywords Acetic acid; CO_2 corrosion; Two-phase horizontal flow

Introduction

Internal localized corrosion is reported to be the predominant failure mechanism of oil and gas pipelines used in transporting crude oil and gas as well as derivative products (Papavinasam et al., 2003). In most cases multiphase flow is encountered, with oil, water, and gas phases arranged in complex patterns. With small quantities of liquids typical for wet gas flow, stratified flow patterns are most common. In these conditions different types of corrosion attack is observed, depending on the part of the pipe. Sun et al. (2000) studied localized CO_2 corrosion in wet gas flow and concluded that it typically occurs at the bottom of the pipe around the iron carbonate saturation point when partially protected film is formed, while the top of the line, which is exposed to pure CO_2 gas and water vapor, experienced little corrosion due to a thin corrosion product film and experienced no localized corrosion.

Top of the line corrosion (TLC) has been reported to exist in a single-phase wet gas line and multiphase gas line with stratified flow regime (Gunaltun and Larrey, 2000; Vitse et al., 2003). The acceleration of TLC is assumed to be the result of competition between the water condensation rate and corrosion rate. The water condensation rate dilutes the condensed water, while the corrosion rate tends to saturate it with corrosion products (Gunaltun and Larrey, 2000).

Address correspondence to P. C. Okafor, Department of Pure and Applied Chemistry, University of Calabar, P. M. B. 1115, Calabar-Nigeria. E-mail: pcokafor@chemist.com

Organic acids, though weak, are known to affect the rate of CO_2 corrosion to a very large extent (Menaul, 1944; Schock and Sudbury, 1951; Obukhova, 1973; Hedges and McVeigh, 1999; Garsany et al., 2002, 2005; Joosten et al., 2002; Guo et al., 2005; Nafday and Nesic, 2005; Singer et al., 2004; Okafor, 2004; Whalley, 1987). These effects are observed on both the top and bottom of the line of pipelines containing multiphase fluids. The quantity of organic acids in produced water in the oil and gas system is in the range of 500 to 3000 ppm (Gunaltun and Larrey, 2000) of which acetic acid contributes 50 to 90% of the organic acids (Obukhova, 1973). Several research articles on the effects of weak organic acids, in particular, acetic acid, on the corrosion of carbon steel in single-phase systems have been reported (Garsany et al., 2002, 2005; Joosten et al., 2002; Guo et al., 2005; Nafday and Nesic, 2005; Singer et al., 2004; Okafor, 2004), but the effects of acetic acid on localized corrosion of carbon steel in a multiphase horizontal flow has not been extensively studied.

The present research is aimed at investigating the effect of acetic acid (concentration range of 500 to 5000 ppm) on CO_2 corrosion of carbon steel in contact with the aqueous and the gaseous phases of two-phase fluid in a low pressure-high temperature horizontal loop.

Experimental Procedures

Description of the Flow Loop

A detailed schematic diagram of the large flow loop developed to accommodate the experimental conditions for this work is shown in Figure 1. The flow loop is a 26 m long, 0.10 m inner diameter, low-pressure, high-temperature system. The entire flow loop is made from 316 stainless steel. A storage tank contains $0.87 \, m^3$ (870.64 L) of 1% NaCl. The tank has 3 KW immersion heaters used for heating the loop. Liquid is moved from the tank by a liquid pump to the progressive cavity pump, which carries the liquid through the system at a fixed superficial liquid velocity of 0.11 m/s and pumps the gas at a fixed velocity of 2 m/s through the system. The liquid serves as a lubricant for the progressive cavity pump as well and the source of liquid phase for the system.

A gas feed line supplies carbon dioxide gas from a 20,000 kg storage tank and maintained the total pressure of the system at 2 bars. An exhaust line with a "knock-out" drum is used to vent gas when required.
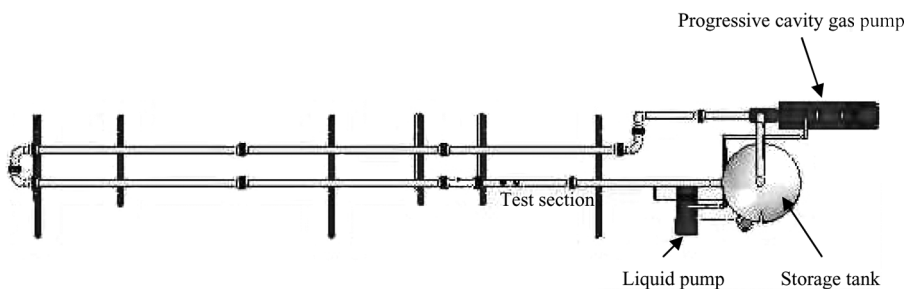
Figure 1. Schematic sketch of the flow loop.

Before experiments were performed with the loop, the system was washed by running diluted HCl solution for 24 hours and then flushed with deionized water until the pH of the water was slightly acidic. Based on long experience with similar equipment, corrosion interference by elements dissolved from the stainless steel surfaces was assumed to be negligible.

Description of the Test Section

Figure 2 (a) and (b) shows the schematic diagram and a cross section of the test section of the flow loop respectively. This section is 0.10 m inner diameter and 2 m long and made from the same material used for constructing the loop. The two ports on the top of the loop (A and B) and one of the ports at the bottom (C) are used for mounting flush-mounted mass loss coupons. The second port at the bottom (D) is used for mounting the linear polarization resistance (LPR) probe for electrochemical measurements. Also at the bottom of the test section are two ports (E) and (F) for inserting a high pressure pH probe and a thermocouple respectively.

Experimental Procedure in Flow Loop

The system was filled with $0.87 \, m^3$ (870.64 L) of the test solution, made up of deionized water +1 mass % (0.1726 M) sodium chloride (NaCl), deaerated by flushing the system with CO_2 until the level of dissolved oxygen fell below 10 ppb. At this level of oxygen, the system is assumed to be saturated with carbon dioxide. The dissolved oxygen level was monitored by using a CHEMet® dissolved oxygen kit. Monitoring the pH was also used to judge when the solution attained equilibrium. The system was then heated to 80°C, pressurized to 2 bar and appropriate amount of acetic acid added. The required amount of acetic acid was first deoxygenated
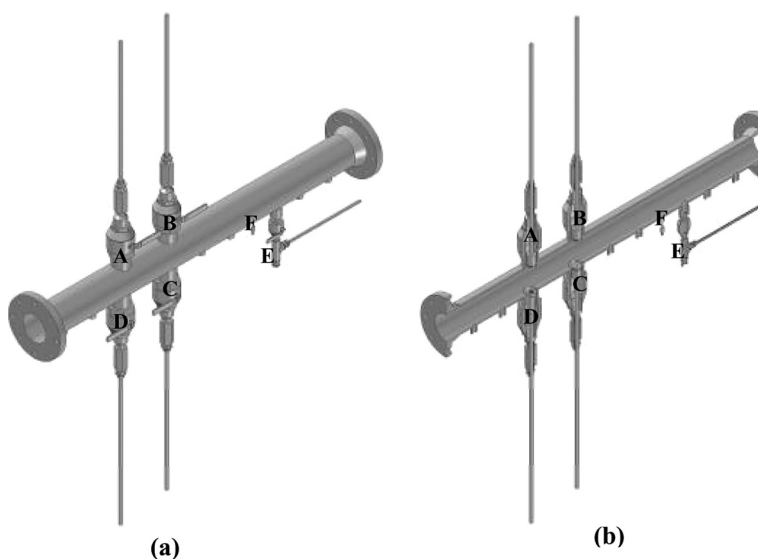
Figure 2. Schematic representation of the (a) test section and (b) cross section of the test section.

before it was introduced into the system using a high-pressure vessel (Singer et al., 2004) and the dissolved oxygen level was monitored to ensure that it fell below 10 ppb. The pH was monitored before and after the acetic acid was added to ensure a constant solution composition. When needed, hydrochloric acid (HCl) or sodium hydrogen carbonate ($NaHCO_3$), calculated from the water chemistry model, was added to adjust the pH. The temperature was maintained within $\pm 1°C$ in all experiments. The flow rates of the gas and liquid were then set and the system allowed to stabilize. The whole procedure takes about 72 hours to attain the desired experimental condition. Once this condition was obtained, the corrosion monitoring probes were inserted into the flow loop.

Mass Loss Measurements

The mass loss coupons used for the loop experiments were circular coupons of cross-sectional area of 0.74 m exposed to the corrodent. They were X 65 carbon steel, used commonly in the construction of oil and gas pipelines, and common construction grade C 1018 carbon steel. The chemical compositions of the steels are shown in Table I. After the exposed period, the coupons were removed from the test section,

Table I. Chemical composition of X 65 and C 1018 carbon steel

Element	Percentage composition (%)	
	X 65	C 1018
Al	0.032	0.001
As	0.008	0.007
B	0.001	0.001
C	0.130	0.160
Ca	0.002	0.007
Co	0.007	0.010
Cr	0.140	0.063
Cu	0.131	0.250
Mn	1.160	0.790
Mo	0.160	0.020
Nb	0.017	0.006
Ni	0.360	0.078
P	0.009	0.008
Pb	<0.001	0.016
S	0.009	0.029
Sb	0.009	0.011
Si	0.260	0.250
Sn	0.007	0.017
Ta	<0.001	0.008
Ti	<0.001	<0.001
V	0.047	0.001
Zr	<0.001	0.004

rinsed in 2-propanol, weighed, and stored in a moisture-free desiccator before surface analysis was carried out. The corrosion rate was calculated from the expression:

$$CR = \frac{m \times 24 \times 365 \times 10}{D \times A \times T} \tag{1}$$

where m is mass loss in grams, D is density in g/cm^3, A is exposed surface area, and T is time of exposure

Electrochemical Measurements

A three-electrode concentric ring probe head (Figure 3) manufactured by Metal Samples$^®$ was used for the loop's electrochemical measurements. The outer ring is made from 316 stainless steel and serves as the counter electrode. The middle and the inner rings are made from C 1018 carbon steel and serve as the working and reference electrodes respectively. Prior to every experiment, the surface of the probe head was polished with 120, 180, 240, 360, 400, and 600 grit silicon carbide paper in succession, rinsed with 2-propanol, then placed in an ultrasonic acetone bath for about 2 minutes to remove possible residue of polishing and air dried. The dried probe head is flush-mounted in the system, and the free corrosion potential was followed immediately until the potential stabilized within ± 1 mV. The solution resistance was then measured using electrochemical impedance spectroscopy (EIS) by applying an oscillating potential of ± 5 mV around the free corrosion potential to the working electrode, using the frequency range of 1 to 100 kHz. The EIS measurement was followed by the polarization resistance (R_p) measurements conducted by polarizing the working electrode ± 5 mV from the free corrosion potential and scanning at 0.1 mV/s. The EC/LPR trend was performed at 60-minute intervals for 168 hours (seven days). The B value used to convert the polarization resistance into a corrosion rate was adopted form the previously conducted small-scale electrochemical study (George et al., 2004).
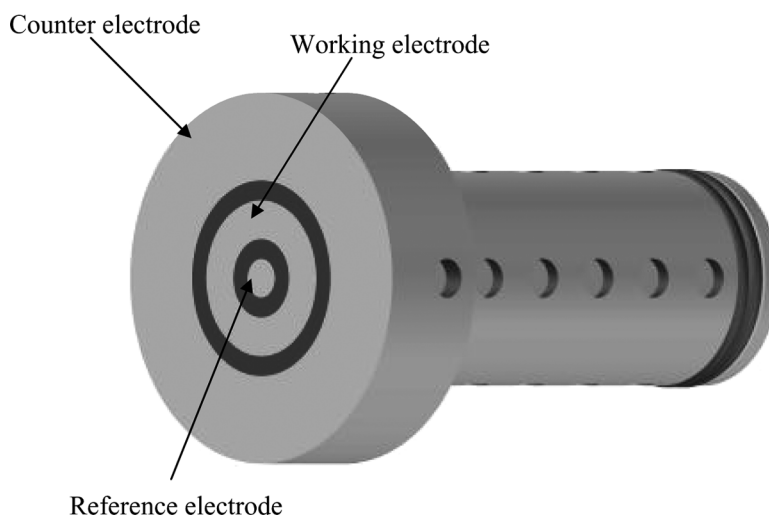
Figure 3. Schematic representation of the electrochemistry probe head showing the three-electrode concentric rings.

Water Chemistry Model

Figure 4 shows a scheme for liquid-gaseous equilibrium when acetic acid and carbon dioxide partition between an aqueous and a gaseous phase. Physical equilibria are superimposed on chemical equilibria. In the aqueous phase the incomplete dissociation of acetic and carbonic acids as well as the dissociation of other species shown in Figure 4 is taken into account. In the gaseous phase, the presence of acetic acid, carbon dioxide, and water vapor is considered. However, it was assumed that ionic species exist only in the aqueous phase and acetic acid dimers can be neglected.

Thus there are three physical equilibrium conditions, that is, for water, carbon dioxide, and monomeric acetic acid:

$$H_2O_{(aq)} \Leftrightarrow H_2O_{(g)} \tag{2}$$

$$CO_{2(aq)} \Leftrightarrow CO_{2(g)} \tag{3}$$

$$CH_3COOH_{(aq)} \Leftrightarrow CH_3COOH_{(g)} \tag{4}$$
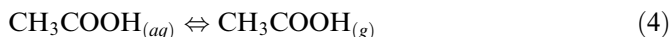
These have to be combined with chemical equilibria: in the liquid phase the formation of carbonic acid and iron carbonate and the dissociation of water, acetic acid, carbonic acid, and hydrogen carbonate ion. It was assumed that there was no complexation with solvent molecules. Furthermore, the mass balance shown in Equation (5)–(7) has to be fulfilled for acetic acid, carbon dioxide, and water. Acetic acid:

$$n_{HAc}^{Tot} = n_{HAc}^{Aq} + n_{Ac^-}^{Aq} + n_{HAc}^{Gas} \tag{5}$$
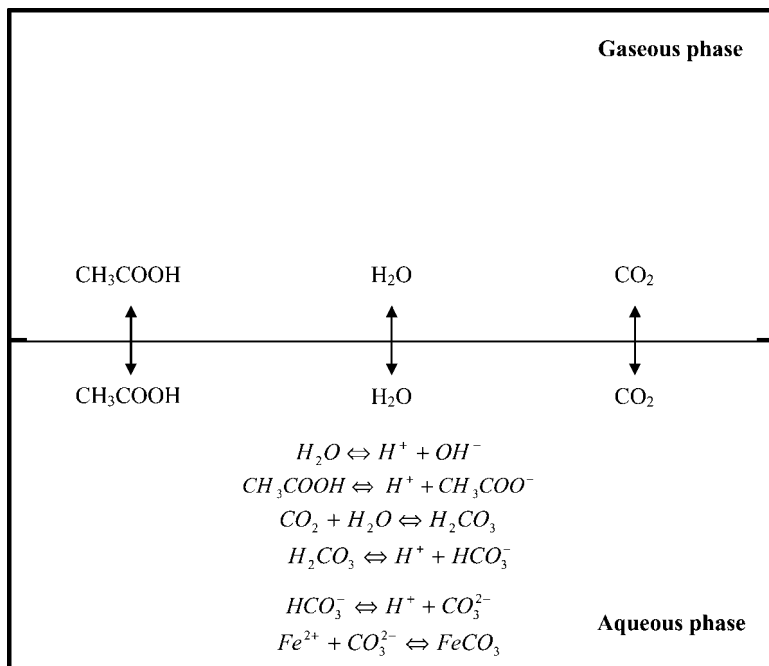
Figure 4. Schematic representation of the liquid-gaseous equilibrium for the acetic acid/water/carbon dioxide system.

Carbon dioxide:

$$n_{CO_2}^{Tot} = n_{CO_2}^{Aq} + n_{H_2CO_3}^{Aq} + n_{HCO_3^-}^{Aq} + n_{CO_3^{2-}}^{Aq} + n_{CO_2}^{Gas} \tag{6}$$

Water:

$$n_{H_2O}^{Tot} = n_{H_2O}^{Aq} + n_{OH^-}^{Aq} + n_{H_2O}^{Gas} \tag{7}$$

The condition for electroneutrality for the aqueous solution results in

$$2[Fe^{2+}] + [H^+] = [Ac^-] + [OH^-] + [HCO_3^-] + 2[CO_3^{2-}] \tag{8}$$

and the total pressure of the system is:

$$P_{Tot} = P_{HAc} + P_{CO_2} + P_{H_2O} \tag{9}$$

Results and Discussion

Bottom of the Line Corrosion

The general corrosion rate at the bottom of the line of the system under study was monitored using mass loss and LPR monitoring techniques, and the results obtained are shown in Figures 5 and 6. From Figure 5, it was observed that general corrosion rate for all concentrations of acetic acid increased slightly with time and then decreased to a stable value ($< 1\,$mm/yr). The slight initial increase is assumed to be due to imperfection on the surface of the metal due to corrosion reaction. This attack changes the surface area of the exposed metal and most likely leads to increase in the electrochemical reactions involved in the reaction process. A similar observation has been reported by Hedges and McVeigh (1999). The observed decrease in corrosion rate with time is due to the formation of corrosion product on the surface of the metal. To confirm this, the LPR probe was removed at the end of each experiment, polished, and reinserted into the same system. As shown in Figure 5,
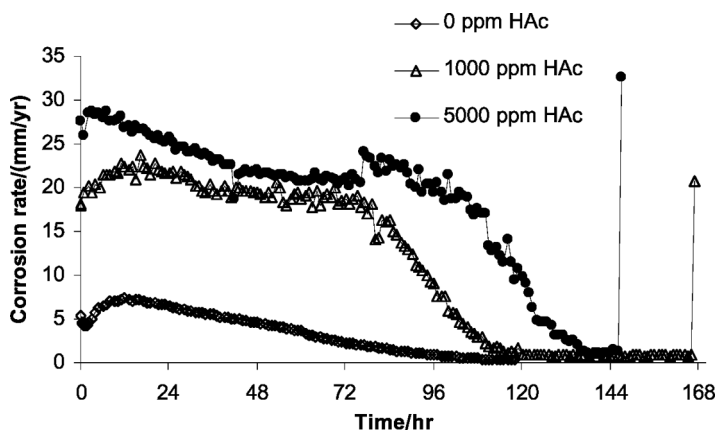
Figure 5. Variation of corrosion rate with time for C 1018 carbon steel in 1% NaCl solution containing different concentrations of total acetic acid at 80°C, 2 bars total pressure, and pH 5.5 at the bottom of the line.
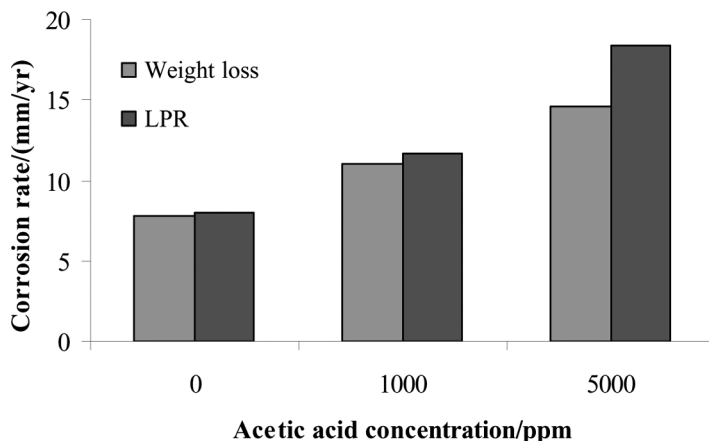
Figure 6. Variation of corrosion rate with total acetic acid concentration from LPR and mass loss methods at the bottom of the line.

the corrosion rate increased to its initial value and the corrosion potential (not shown) dropped to the starting potential. Visual observation of the LPR probe after each test revealed that the surface was completely covered with dark-gray, almost black corrosion product. Sun et al. (2000) reported similar findings. Analysis of the product on this coupon was however not carried out. Comparing the integrated LPR and mass loss results (Figure 6) showed that the corrosion rate for the X 65 carbon steel and the LPR probe gave similar results.

Effect of Acetic Acid
The presence of acetic acid was observed to increase the rate of general corrosion. This observation is in line with those previously reported (Sun et al., 2003; Garsany et al., 2002; Joosten et al., 2002; Okafor, 2004; Whalley, 1987), and is known to be due to the effect of undissociated acetic acid on the cathodic reactions of the corrosion process (Okafor, 2004; Whalley, 1987). The calculated concentration of undissociated acetic acid for the system studied is shown in Table II. Increase in undissociated acetic acid, as shown in Figures 5 and 6, increased the corrosion rate

Table II. Equilibrium concentrations of undissociated acetic acid in liquid and gas phases at 80°C, 2 bars total pressure, and pH 5.5

Total (ppm)	Undissociated acetic acid (ppm)	
	Liquid phase	Gas phase $\times 10^{-9}$
10	1.87	6.89
100	18.74	68.88
500	93.70	344.85
1000	187.40	688.97
2500	468.49	1722.42
5000	936.98	3448.50
10000	1873.95	6889.70

of the C 1018 and X 65 carbon steel due to the increase in the contribution of acetic acid to the hydrogen reduction process of the cathodic reaction (Singer et al., 2004).

Surface Analysis of the Coupon

The corrosion product and surface of the X 65 carbon steel coupon were analyzed using scanning electron microscopy (SEM) and x-ray diffraction (XRD). The SEM micrograph is shown in Figure 7. The films were soft and very easy to remove with Clarke's Solution, used for removing the corrosion products on the carbon steel surface before final mass loss measurements (Haynes and Baboian, 1983). X-ray diffraction spectroscopic analysis on the deposited substances, shown in Figure 8, confirmed them to be predominantly iron carbide. The latter is the "skeleton," i.e., the uncorroded portion of carbon steel remaining after anodic dissolution of the ferrite phase. The findings are in good agreement with previous investigations (Van Hunnik, 1996;
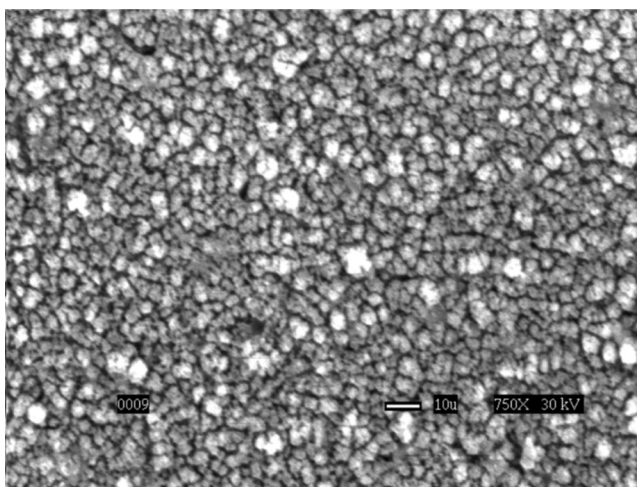
Figure 7. SEM surface analysis of the corrosion product on X 65 carbon steel.
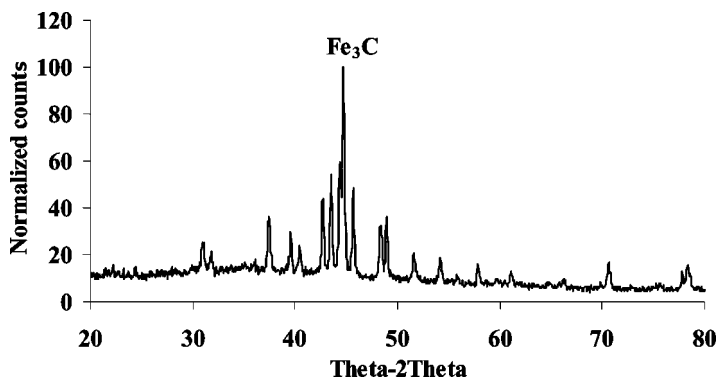
Figure 8. XRD spectrum for corrosion product on the bottom of the line for X 65 carbon steel in 1% NaCl solution containing 1000 ppm total acetic acid.

Nesic and Lee, 2003) conducted in this range of pH. After carefully removing the film and viewing the surface of the specimen with a metallurgical microscope, no localized corrosion was observed.

Top of the Line Corrosion

Mass loss measurements were conducted only on the top of the line. This is because electrochemical measurements have been reported to fail on top of the line corrosion studies because of the low conductivity of the condensed water (Nesic et al., 1996). For this experiment, C 1018 and X 65 carbon steels were used, and the corrosion measurements results obtained are shown in Figure 9. Figure 9 shows the variation of general corrosion rate with acetic acid concentration for C 1018 and X 65 carbon steel in 1% NaCl solution containing different concentrations of acetic acid at 80°C, 2 bars total pressure, and pH 5.5 on the top of the line. It was observed that increase in acetic acid increased the corrosion rates remarkably, and the corrosion rates for both metals were very close, although the corrosion rate of the C 1018 carbon steel was slightly higher than that of the X 65 carbon steel. A similar trend was also observed for the bottom of the line, as shown in Figure 6.

Figures 10 and 11 show photographs of the coupons taken immediately after removal of the coupons from the test solution. Visual observations show that a greater amount of attack was within a concentric shape presumed to be the area of dropwise condensation. The size of this concentric shape increased with increase in acetic acid concentration, as shown in Figure 12. This is most likely due to the fact that increase in acetic acid increases the concentration of undissociated acetic acid in the droplet and thus increases the concentration of acetic acid in contact with the metal surface and may also be due to a greater retention time of the droplets, containing acetic acid, on the surface of the metal.

The surfaces of the specimen were analyzed before and after removal of the corrosion products. The results of these analyses are as shown in Figure 13 and 14. It was observed that iron carbonate crystals were selectively precipitated on the surface of the metal. This shows that the droplets in contact with the surface of the
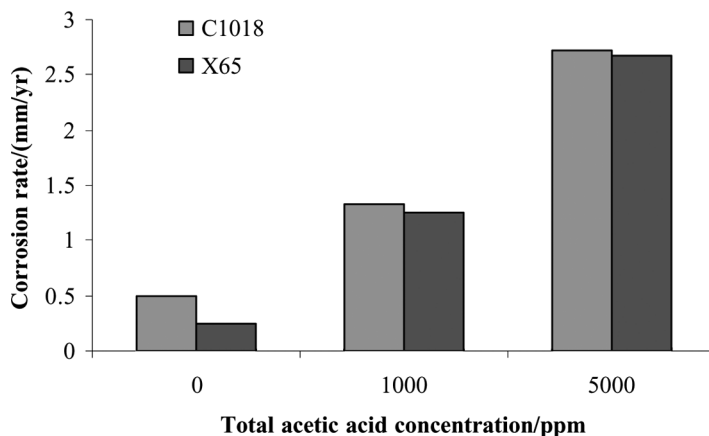
Figure 9. Variation of corrosion rate with concentration of total acetic acid for C 1018 and X65 carbon steel.
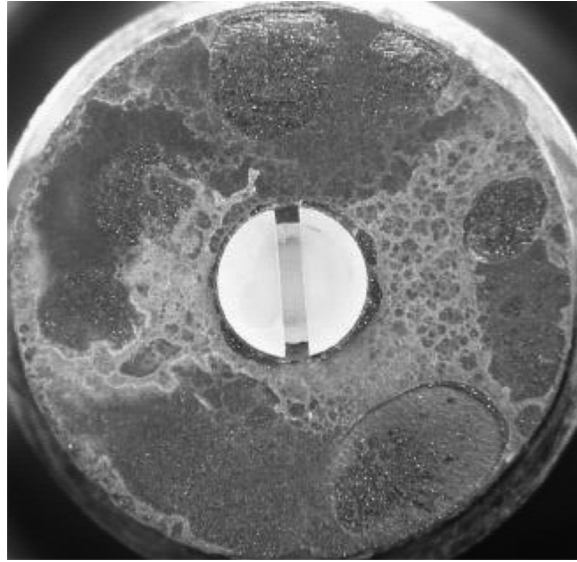
Figure 10. Photo of X 65 carbon steel coupon on top the of the line after 168 h of exposure in the presence of 1000 ppm total acetic acid.

metal are saturated with corrosion products that lead to conditions necessary for precipitation of iron carbonate crystals. XRD analysis, shown in Figure 15, confirmed that iron carbonate was the predominant product formed under the present test condition.

Figure 11. Photo of X 65 carbon steel coupon on the top of the line after 168 h of exposure in the presence of 5000 ppm total acetic acid.
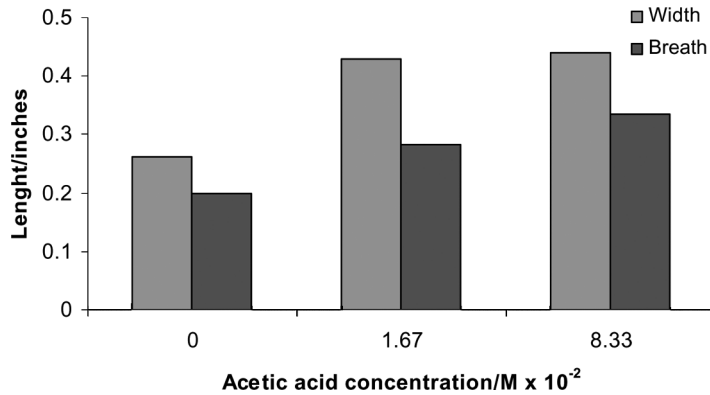
Figure 12. Variation of droplet width and breath with concentration of acetic acid for X 65 carbon steel exposed to CO_2 saturated solution for 168 h at pH 5.5, 80°C, Vsl 0.11 m/s, and Vsg 2 m/s on top of the line.

From Figure 14, it is observed that the local precipitation of iron carbonate on the droplets resulted in the initiation of localized attack at sites between the iron carbonate film and the unprotected region.

In a flowing system or wet gas lines, top of the line corrosion has been observed in pipelines (Gunaltun and Larrey, 2000; Vitse et al., 2003). This type of corrosion is assumed to be due to condensation of water and condensable gases present in the system. Noncondensable gases, like CO_2, present in the system are assumed to be in equilibrium with the condensed liquid in a way similar to the liquid on bottom of the line.

The nature of the corrosion on the top of the line depends greatly on the type, size, and retention time of the condensed liquid on the surface of the metal. Condensation can occur in two ways; filmwise condensation, where the condensate forms a
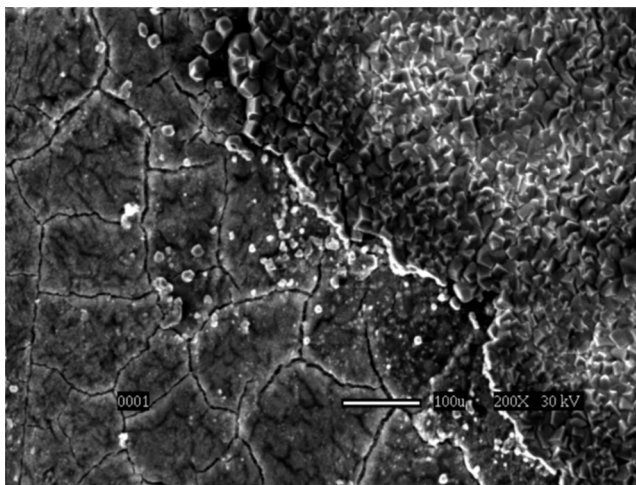
Figure 13. SEM micrograph of selective precipitation of iron carbonate crystals on X 65 carbon steel in CO_2 saturated solution for 168 h in the absence of acetic acid at pH 5.5, 80°C, Vsl 0.11 m/s, and Vsg 2 m/s on the top of the line.

(a)
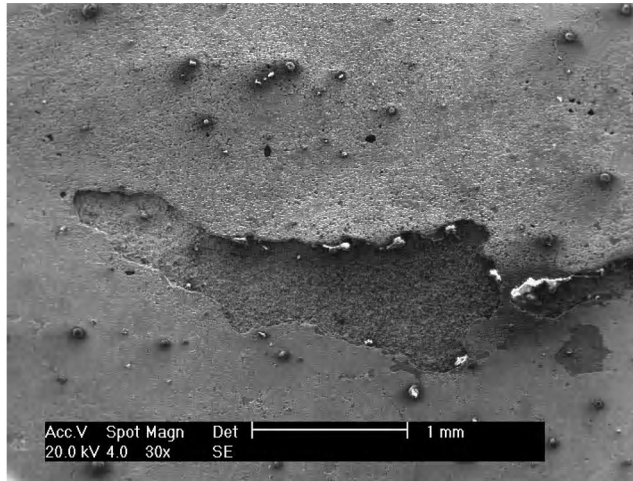
(b)

Figure 14. (a) Photograph of X-65 carbon steel after removal of film for coupon exposed in CO$_2$ saturated solution for 168 h in the absence of acetic acid at pH 5.5, 80°C, Vsl 0.11 m/s, and Vsg 2 m/s on the top of the line and (b) SEM micrograph of the circled area showing localized corrosion.

continuous film on the solid surface, and dropwise condensation, in which the condensate forms in drops that do not wet the entire solid surface well. The drops therefore do not form a continuous film; instead they reach a certain critical size and then run off or drop off the surface. The surface is left ''dry'' and another drop can begin to form (Sadhal et al., 2004). As was observed on the coupons in Figures 10 and 11, the topographical variations on the surface of the metal suggest that dropwise condensation dominated on the top of the line for the systems under study.
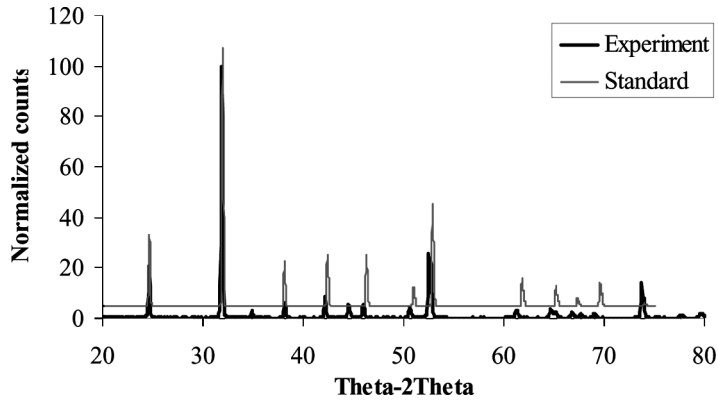
Figure 15. XRD spectrum for corrosion product on the top of the line for X 65 carbon steel in 1% NaCl solution containing 1000 ppm acetic acid.

In dropwise condensation, the droplet is in direct contact with the surface of the metal and due to the dissolved CO_2 and, in the presence of acetic acid, the undissociated acetic acid, the corrosion on the surface of the metal at the points of contact with the metal surface will be initially higher than that on the other areas without droplets. During the process of corrosion, protons (H^+) are reduced and iron is oxidized, leading to a ferrous ion (Fe^{2+}) release into the condensed droplets (as shown in Figure 16), and this increases the pH. The increase in pH results in higher supersaturation by iron carbonate, know to be the driving force for the precipitation rate of iron carbonate (Haynes and Baboian, 1983; Dugstad, 1992; Nesic and Lunde, 1994; Sun, 2003):

$$Fe^{2+} + CO_3^{2-} \Leftrightarrow FeCO_3 \qquad (10)$$

Increase in pH in the droplet also changes the speciation of species in the droplet and changes the mechanism of electrochemical reactions at the wall (Dugstad, 1992). The precipitated iron carbonate crystals deposit on the surface of the metal. The crystal
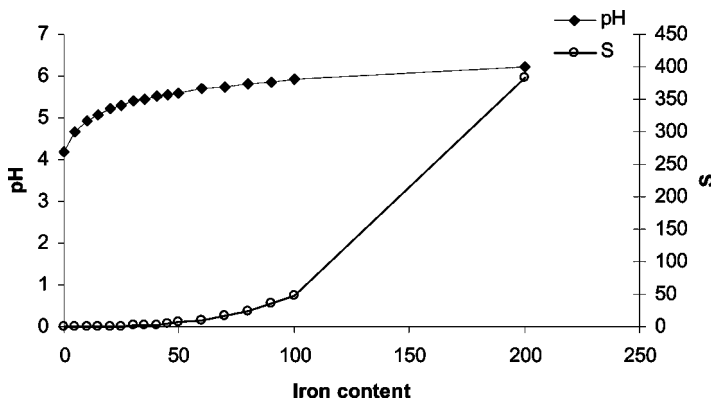
Figure 16. Effect of iron content on pH and supersaturation at 80°C and 1 bar CO_2 generated from the water chemistry model.
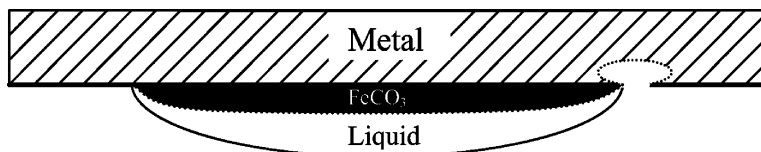
Figure 17. Schematic of a dropwise condensation showing the precipitated iron carbonate and the initiation of localized corrosion at the site between the protected and nonprotected regions during TLC.

serves two purposes: it protects the surface of the metal from further corrosion and also creates a rough surface beneath the droplet, which plays a very important role in the adherence and retention time of the droplet, and thus on the precipitation of more iron carbonate crystals.

The local precipitation of iron carbonate beneath the droplets results in the initiation of localized attack at sites between the iron carbonate film and the unprotected region. It is assumed here that a galvanic cell is probably set up between the film-free region (which serves as the anodic part) and the film protected region (which serves as the cathodic). This view is also held by others (Dugstad, 1992; Nesic and Lunde, 1994). This results in a high corrosion rate in the site between the iron carbonate film and the unprotected region. Once localized corrosion is initiated, the base of the more attacked region becomes anodic with respect to the more noble iron carbonate film region, and, thus, more localized attack progresses beneath the protected region near the edge, as demonstrated in Figure 17. However, the exact conditions under which this localized attack is formed are still being investigated.

When a gaseous acetic acid is present in a multiphase system, two effects may likely occur. First, it may adsorb, like most organic substances, on the surface of the metal and help promote dropwise condensation (Sadhal et al., 1997) and second it may dissolve in the formed droplet and dissociate into protons and acetate ions:

$$CH_3COOH \Leftrightarrow H^+ + CH_3COO^- \tag{11}$$

The undissociated acetic acid is reduced at the surface of the metal by supplying the protons, which accelerates the cathodic reaction and the local corrosion rate (Garsany et al., 2005; Okafor, 2004; Whalley, 1987).

Conclusions

- Long-term large-scale corrosion experiments that faithfully represent combined CO_2/organic acid corrosion attack seen in the field have been conducted. For the first time, anecdotal field experience, suggesting that the presence of organic acids can aggravate localized attack at the top of the line in stratified flow, was confirmed in controlled laboratory experiments.
- The presence of acetic acid increases the general CO_2 corrosion rate of carbon steel with increase in concentration for both bottom and top of the line coupons.
- The nature of the corrosion on the top of the line depends on the type, size, and retention time of the condensed droplets.

- The local precipitation of iron carbonate beneath droplet condensations results in the initiation of localized attack at sites between the iron carbonate firm and the unprotected region.
- The presence of acetic acid on top of the line corrosion increases the corrosion rate by promoting dropwise condensation, increasing size and retention time and accelerating the corrosion rate due to its effects on the cathodic reaction.

Acknowledgments

References

Dugstad, A. (1992). The importance of $FeCO_3$ supersaturation on the CO_2 corrosion of carbon steels, Paper no. 14 presented at CORROSION/92.

Garsany, Y., Pletcher, D., and Hedges, B. (2002). *J. Electroanal. Chem.*, 538–539: 285–297.

Garsany, Y., Pletcher, D., Sidorin, D., and Hedges, W. M. (2005). *Corrosion*, **60**(12), 1155–1167.

George, K., Nesic, S., and de Waard, C. (2004). Electrochemical investigation and modeling of carbon dioxide corrosion of carbon steel in the presence of acetic acid, Paper presented at CORROSION/2004.

Gunaltun, Y. M. and Larrey, D. (2000). Correlation of cases of top of the line corrosion with calculated water condensation rates. Paper no. 00071 presented at CORROSION/2000.

Guo, P., Chen, Z. Y., Liu, D., Bando, K., and Tomoe, Y. (2005). The effect of acetic acid and acetate on CO_2 corrosion of carbon steel, Paper no. 05306 presented at CORROSION/ 2005.

Haynes, G. S. and Baboian, R. (1983). *Laboratory Corrosion Tests and Standards*, American Society for Testing and Materials, Philadelphia.

Hedges, B. and McVeigh, L. (1999). The role of acetate in CO_2 corrosion: The double whammy, Paper no. 21 presented at CORROSION/1999.

Joosten, M. W., Kolts, J., and Hembree, J. W. (2002). Organic acid corrosion in oil and gas production, Paper no. 02294 presented at CORROSION/2002.

Menaul, P. L. (1944). Causative agents of corrosion in distillate field, *Oil Gas J.*, **43**(27), 80–81.

Nafday, O. A. and Nesic, S. (2005). Iron carbonate film formation and CO_2 corrosion in the presence of acetic acid, Paper no. 05295 presented at CORROSION/2005.

Nesic, S. and Lee, K.-L. J. (2003). *Corrosion*, **59**(7), 616–628.

Nesic, S. and Lunde, L. (1994). Carbon dioxide corrosion of carbon steel in two-phase flow, *Corrosion*, **50**(9), 717.

Nesic, S., Postlethwaite, J., and Olsen, S. (1996). *Corrosion*, **52**(4), 280–294.

Obukhova, Z. P. (1973). Candidates dissertation VN11GAZ, Moscow, 1974, *Gazovaya Promyshlennost*, number 4, 48.

Okafor, P. C. (2004). *Investigation and modelling of carbon (iv) oxide corrosion of carbon steel in the presence of acetic acid*, Ph.D. diss., University of Calabar, Calabar, Nigeria.

Papavinasam, S., Revie, R. W., Attard, M., Demoz, A., and Michaelian, K. (2003). *Corrosion*, **59**(12), 1096–1111.

Sadhal, S. S., Ayyaswamy, P. S., and Clung, J. N. (1997). *Transport Phenomena with Drops and Bubbles*, Springer, New York.

Schock, D. A. and Sudbury, J. D. (1951). Prediction of corrosion in oil and gas wells, *World Oil*, **133**(5), 180–184.

Singer, M., Nesic, S., and Gunaltun, Y. (2004). Top of the line corrosion in the presence of acetic acid and carbon dioxide, Paper no. 04377 presented at CORROSION/2005.

Sun, Y. (2003). Localized CO_2 corrosion in horizontal wet gas flow, Ph.D. diss., Dept. of Chemical Engineering, Ohio University, Athens, Ohio.

Sun, Y., George, K., and Nesic, S. (2000). The effect of chloride and acetic acid on localized CO_2 corrosion in wet gas flow. Paper no. 03327 presented at CORROSION/2003.

Van Hunnik, E. W. J. (1996). The formation of protective $FeCO_3$ corrosion product layers in CO_2 corrosion, Paper no. 6 presented at CORROSION/96.

Vitse, F., Nesic, S., Gunaltun, Y., Larrey de Torreben, D., and Duchet-Suchaux, P. (2003). *Corrosion*, **59**(12), 1075–1085.

Whalley, P. B. (1987). *Boiling, Condensation, and Gas-Liquid Flow*, Clarendon Press, Oxford.